

1 On the application of the beam model for linear dynamic
2 analysis of pile and suction caisson foundations for offshore
3 wind turbines*

4 Guillermo M. Álamo[†], Jacob D.R. Bordón, Juan J. Aznárez

5 Instituto Universitario de Sistemas Inteligentes y Aplicaciones Numéricas en Ingeniería (SIANI), Universidad de Las
6 Palmas de Gran Canaria, Edificio Central del Parque Científico y Tecnológico, Campus Universitario de Tafira, 35017 Las
7 Palmas de Gran Canaria, Spain

8 **Abstract**

9 Piles and suction caissons are the most common foundation solutions for fixed Offshore Wind Turbines
10 at intermediate water depths. They are generally used as a single element, presenting large diameters and
11 short aspect ratios. These specific dimensions drastically differ from the ones of classical applications (off-
12 shore platforms, bridges, tall buildings etc.). Thus, in this paper the validity of their modelling as beam
13 elements for the particular problem of OWT is revised. The results of a soil-beam model, based on the integral
14 Reciprocity Theorem in Elastodynamics and specific Green's functions for the layered half-space for the soil
15 behaviour coupled with Timoshenko's beam Finite Elements, are benchmarked against the ones of a soil-shell
16 model, based on Boundary Elements for the soil coupled with shell Finite Elements. The comparative study
17 is conducted in terms of foundation characterization variables (impedance functions and kinematic interaction
18 factors). Their influence on the OWT seismic response is also studied through a substructuring procedure.
19 From the results, some expressions for determining the applicability range of the beam simplification are pro-
20 posed as functions of the relative foundation-soil stiffness ratio. It is observed that this applicability range
21 goes beyond that the one commonly considered.

22 **Keywords:** Offshore Wind Turbine; Suction Caisson Foundation; Monopile Foundation; Seismic Re-
23 sponse; Boundary Elements; Finite Elements

*Pre-print of the paper published in COMPUTERS AND GEOTECHNICS, 134, 104107 (2021), DOI:
<https://doi.org/10.1016/j.compgeo.2021.104107>

[†]Corresponding Author. E-mails: {guillermo.alamo, jacobdavid.rodriguezboron, juanjose.aznarez}@ulpgc.es

24 **Contents**

25 **1 Introduction** **3**

26 **2 Methodology** **5**

27 2.1 Substructuring model 5

28 2.2 Soil-shell model 7

29 2.3 Soil-beam model 9

30 **3 Results and discussion** **11**

31 3.1 Static stiffnesses 12

32 3.2 Impedance functions 14

33 3.3 Kinematic interaction factors 16

34 3.4 Expressions for the limiting frequencies 16

35 3.5 Application example 18

36 **4 Conclusions** **20**

37 **A Validity of J as characteristic dimensionless parameter for dynamic analyses** **26**

1 Introduction

Pile and suction caisson foundations (also known as buckets, suction piles or suction anchors depending on the context) are being used as foundations of fixed Offshore Wind Turbines (OWT). Such solutions are being considered at sites with shallow (10 to 30 meters) and intermediate water depths (30 to 60 meters) with single (monopile or monobucket) or multiple foundation arrangements depending on both water depth and soil properties.

As wind turbines becomes larger, the required piles and suction caissons becomes bigger in diameter: up to 8 meters for monopiles (XXL monopiles), up to 30 meters for caissons [Cotter, 2009], and even bigger for shallow composite caissons with internal skirts (see e.g. [Jia et al., 2018]). Such diameters are much bigger than diameters used in other more classical projects (gas/oil platforms, bridges, buildings, etcetera), and therefore the use of models traditionally considered should be taken with care. The length L to diameter D ratios ranges are $3 < L/D < 10$ for monopiles and $1 < L/D < 6$ for suction caissons [Houlsby and Byrne, 2005a, Houlsby and Byrne, 2005b]. The buried part of both piles and caissons are constituted by steel shells of thickness around $t/D \sim 0.01$ (pile shaft) for monopiles and $t/D \sim 0.001$ (caisson skirt) for suction caissons.

The complete design of an OWT is a complex task which should fulfil many requirements [DNV, 2014]. Although rough designs can be obtained from simplified procedures at early stages, see e.g. [Arany et al., 2017], final designs should be defined after using an integrated optimization procedure which guarantees a safe and economical solution, see e.g. [Ashuri et al., 2014]. In this sense, it is of fundamental importance an appropriate modelling which should also be computationally efficient due to the many evaluations needed during the design process. In the case of foundation modelling, recent works [Bhattacharya et al., 2013, Bordón et al., 2019, Page et al., 2019], have highlighted its importance particularly for the prediction of first and second natural frequencies, which are relevant for performing the crucial fatigue analyses. In the case of seismic analyses, the frequency range usually goes far beyond the second natural frequency. The use of convenient simplifying hypotheses allows adopting simpler and cheaper models (ideally via closed-form formulae or calibrated fast models) at initial steps, whereas more rigorous, complex and detailed models should be considered at the final stages.

The present paper is concerned with the modelling of big diameter and short piles and suction caissons for seismic analyses of OWT supported by a single foundation element (monopile or monobucket). The focus is put on assessing the adequacy of different simplifying hypothesis which allow the use of more elementary models from which results are more easily obtained. To this end, a previously developed soil-beam coupled model [Álamo et al., 2016] is compared against a rigorous soil-shell model [Bordón et al., 2017]. The former

69 is a model which reduces the soil-structure interaction to a line (pile axis), and greatly reduces the number
70 of degrees of freedom. The pile itself is modelled with Timoshenko finite elements, and the soil response is
71 included via Green's function for an arbitrary horizontally layered half-space, which avoid the discretisation
72 of the free-surface and the layer interfaces, i.e. only pile axis nodes are present. The latter model reduces the
73 soil-structure interaction to the shell mid-surface, which leads to a rigorous and general interaction model but
74 it is also computationally costlier. The comparative study is performed in terms of impedances and kinematic
75 interaction factors. In addition to this, results in terms of OWT variables are also compared in order to evaluate to
76 what extent the differences in the foundation modelling are transmitted to the whole tower-supporting structure-
77 foundation system.

78 The use of some kind of one-dimensional reduction, i.e. beam-like models, for foundation modelling is
79 quite advantageous for obvious mathematical and computational reasons. The key of such models is how
80 soil-structure interaction is considered. Pioneering works take the rigorous Mindlin's solution and integrate
81 it along the pile axis or pile shaft under certain assumptions (see e.g. [Jiménez-Salas and Belzunce, 1965,
82 Thurman and D'Appolonia, 1965, Poulos and Davis, 1968]). An alternative approach is the well-known Win-
83 kler model, where distributed springs and dashpots are connected along the pile axis [Novak et al., 1978, Gazetas and Dobry, 1984].
84 Advanced approaches use some Green's function under point or ring loading to introduce the soil response,
85 and then this is coupled to beam finite elements in different ways [Kaynia and Kausel, 1982, Coda et al., 1999,
86 Almeida and de Paiva, 2004, Padrón et al., 2007]. The soil-beam model used in this paper extends [Padrón et al., 2007]
87 by considering an arbitrary horizontally layered half-space and Timoshenko finite elements. The aim of the
88 present work is to study to what extent this soil-beam model, initially developed for pile foundations, is able to
89 reproduce soil-structure interaction (impedances and kinematic interaction factors) for length to diameter ratios
90 as low as 1, i.e. suction caissons.

91 The paper is organized as follows. First, Section 2 presents the two different foundation models together
92 with the substructuring model used to compute the OWT system response. Then, the comparison between the
93 beam and shell models is conducted along the different parts of Section 3. The comparison starts in terms of
94 the foundation response: static (Sec. 3.1) and dynamic (Sec. 3.2) stiffness, and kinematic interaction factors
95 (Sec. 3.3). Then, some expressions determining the upper frequencies below which the beam model accurately
96 reproduces the foundation response are proposed in Sec. 3.4. The final part of the comparison, in terms of
97 OWT variables, is done through the application example presented in Sec. 3.5. The paper ends listing the main
98 conclusions drawn from the study in Section 4.

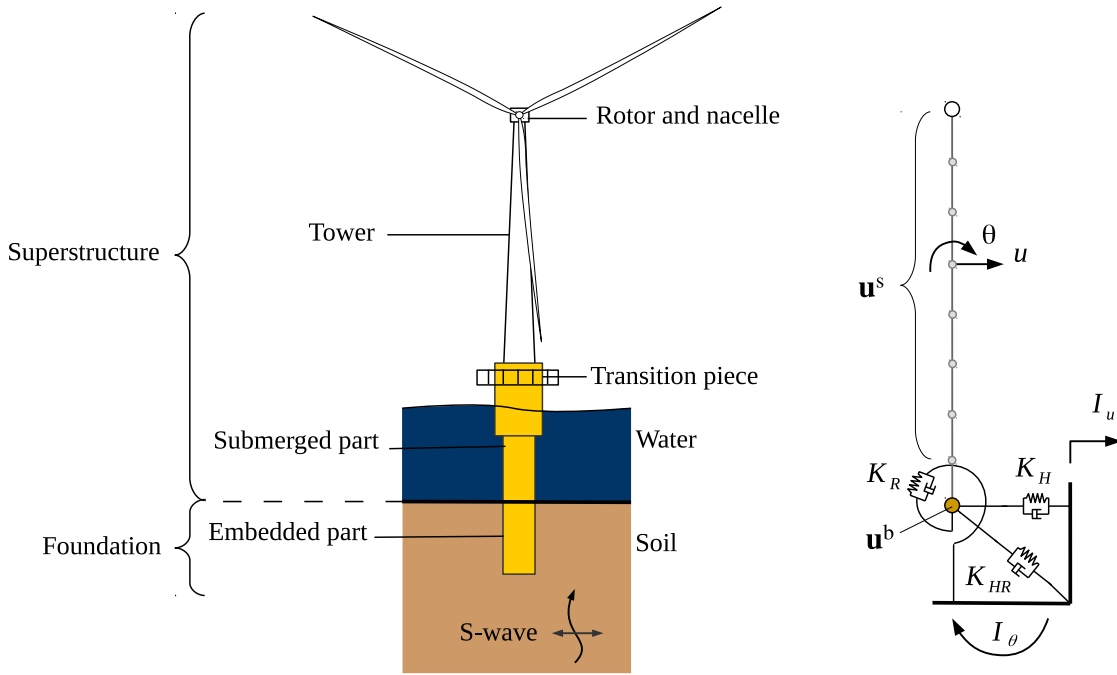


Figure 1: Problem layout and substructuring model

2 Methodology

2.1 Substructuring model

The problem at hand is summarized in Fig. 1: an Offshore Wind Turbine connected to a submerged structure founded on a large diameter and relatively short monopile or suction caisson subjected to vertically-propagating S waves.

A two-dimensional (lateral behaviour) substructuring model is used for modelling the OWT dynamics. It comprises a simple concentrated mass at the hub representing the Rotor-Nacelle-Assembly (RNA), a sufficient number of Euler-Bernoulli beam elements for taking into account the conical tower and the submerged part. The foundation dynamics is synthesized via frequency dependent springs and dashpots (impedance functions) connected to the submerged part base. The foundation energy filtering when impinged by a seismic action (vertically incident shear waves) is taken into account via kinematic interaction factors. An adequate representation of both impedances and kinematic interaction factors is vital for the study of OWT modal and seismic behaviour.

The impedance functions relate the forces and moments and the displacements and rotations of the foundation at the mudline level. They are frequency-dependent complex functions whose real and imaginary parts represent respectively the stiffness and damping characteristics of the foundation. Given that the study focuses on the lateral behaviour, only horizontal K_H , rocking K_R and sway-rocking cross-coupling K_{HR} impedance func-

115 tions are considered in the substructuring formulation. However, the vertical stiffness term K_V is also analysed
 116 in this work when studying the foundation-only response.

117 The kinematic interaction factors represent the filtering effects of the foundation, and they are computed as
 118 the ratio between the displacement or rotation at the foundation and the free-field motion at the mudline. The
 119 translational and rotational kinematic interaction factors are respectively denoted as I_u and I_θ .

120 More details about the methodologies (soil-shell or soil-beam) used to evaluate the impedance functions and
 121 kinematic interaction factors are given in next sections. In both models, a time harmonic analysis at circular
 122 frequency ω is considered, and the soil is assumed to be a homogeneous linear elastic solid with following
 123 properties: shear modulus G_s , Poisson's ratio ν_s , density ρ_s and hysteretic damping ratio ξ_s ; being the complex
 124 effective shear modulus to be used $G_s^* = G_s(1 + i2\xi_s)$.

125 The governing equations in the frequency-domain that are used to obtain the system response can be written
 126 as:

$$\left(\begin{bmatrix} \mathbf{K}^{ss} & \mathbf{K}^{sb} \\ \mathbf{K}^{bs} & \mathbf{K}^{bb} + \mathbf{K}^f \end{bmatrix} - \omega^2 \begin{bmatrix} \mathbf{M}^{ss} & \mathbf{M}^{sb} \\ \mathbf{M}^{bs} & \mathbf{M}^{bb} \end{bmatrix} \right) \begin{Bmatrix} \mathbf{u}^s \\ \mathbf{u}^b \end{Bmatrix} = \begin{Bmatrix} \mathbf{0} \\ \mathbf{F}^b \end{Bmatrix} \quad (1)$$

127 where \mathbf{u} is the vector containing nodal in-plane lateral displacements and rotations, \mathbf{K} and \mathbf{M} are the stiffness
 128 and mass matrices of the system obtained by assembling the elementary ones, the indexes distinguish between
 129 all structural nodes (s) and the base (mudline level) one (b), \mathbf{K}^f is the impedance matrix of the foundation, and
 130 \mathbf{F}^b is the force and moment acting at the base of the structure due to the seismic excitation. This force vector
 131 can be computed from the impedance matrix and kinematic interaction factors as:

$$\mathbf{F}^b = [\mathbf{K}^f] \begin{Bmatrix} I_u \\ I_\theta \end{Bmatrix} \quad (2)$$

For comparison purposes, the response of the system neglecting Soil-Structure Interaction (SSI) effects is
 also considered, i.e. rigid base assumption. In this case, the free field motion u_{ff} is directly introduced at the
 mudline node of the superstructure, while restricting its rotation. This simplification reduces Eq. (1) into:

$$(\mathbf{K}^{ss} - \omega^2 \mathbf{M}^{ss}) \mathbf{u}^s = -(\mathbf{K}^{sb} - \omega^2 \mathbf{M}^{sb}) \mathbf{u}^b, \quad \text{being: } \mathbf{u}^b = \begin{Bmatrix} 1 \\ 0 \end{Bmatrix} u_{ff} \quad (3)$$

2.2 Soil-shell model

The monopile shaft and the suction caisson skirt are topologically similar, and the only differences are the dimensions of the foundation element. In both cases the thickness to diameter ratios t/D are well below 5%, being smaller in the case of suction caissons skirts (typically $t/D \sim 0.001$) than in the case of monopile shafts (typically $t/D \sim 0.01$). The consideration of a purely continuum three-dimensional solid model for the soil-foundation system is therefore unnatural and overly complex. Instead, the monopile shaft or suction caisson skirt is more appropriately modeled as a shell, leading to a mixed dimensional model which considerably reduces the required number of degrees of freedom.

Such a model has been developed by the Authors [Bordón et al., 2017] via a BEM-FEM approach which considers the interaction between the foundation and the soil as the interaction of a shell (FEM) and the surrounding soil (BEM), see Fig. 2. The main hypothesis of this model is thus the reduction of soil-shell interaction to the mid-surface of the shell. The present model is fully described for the case of Biot's poroelastic soils in [Bordón et al., 2017], but a brief description of the this model for an elastic soil is outlined below.

The soil domain Ω_s is discretized by using the BEM, which is based on the use of Boundary Integral Equations (BIE) relating displacements u_k and tractions t_k throughout its boundary $\Gamma = \partial\Omega_s$. The boundary Γ consists of two parts: free-surface boundary Γ_{fs} , and shell mid-surface Γ_{shm} considered as a crack-like boundary ($\Gamma_{shm} = \Gamma_{shm}^+ + \Gamma_{shm}^-$). The Singular BIE is used for collocating along the free-surface Γ_{fs} [Domínguez, 1993]:

$$c_{lk}^i u_k^i + \int_{\Gamma} t_{lk}^* u_k \, d\Gamma = \int_{\Gamma} u_{lk}^* t_k \, d\Gamma \quad (4)$$

where $l, k = 1, 2, 3$ and the Einstein summation convention is implied. The tensor c_{lk}^i is the free-term at the collocation point, u_k^i is the displacement at the collocation point, and u_{lk}^* and t_{lk}^* are the elastodynamic fundamental solutions in terms of displacements and tractions respectively. The Dual (Singular and Hypersingular) BIEs are used for collocating on the shell mid-surface Γ_{shm} :

$$\frac{1}{2} (u_l^{i+} + u_l^{i-}) + \int_{\Gamma} t_{lk}^* u_k \, d\Gamma = \int_{\Gamma} u_{lk}^* t_k \, d\Gamma \quad (5)$$

$$\frac{1}{2} (t_l^{i+} - t_l^{i-}) + \int_{\Gamma} s_{lk}^* u_k \, d\Gamma = \int_{\Gamma} d_{lk}^* t_k \, d\Gamma \quad (6)$$

where u_k^{i+}, t_k^{i+} and u_k^{i-}, t_k^{i-} are displacements and tractions at the collocation point along respectively the positive and negative crack faces, and d_{lk}^* and s_{lk}^* are obtained from the differentiation of u_{lk}^* and t_{lk}^* (see e.g.

147 [Domínguez et al., 2000]). In Eqs. (5-6), it has been assumed that the collocation point \mathbf{x}^i is located at a smooth
 148 boundary point ($\Gamma_{\text{shm}}(\mathbf{x}^i) \in \mathcal{C}^1$) leading to the 1/2 factor present in them. This assumption is related to the
 149 required use of \mathcal{C}^1 geometric continuity at collocation points for Hypersingular BIEs. In order to overcome
 150 this, the Multiple Collocation Approach (MCA) [Ariza and Domínguez, 2002] is used when collocating at a
 151 crack boundary point. Standard quadratic triangular (6 nodes) and quadrilateral (9 nodes) boundary elements
 152 are considered for the discretization.

The shell region Ω_{sh} is discretized by using the FEM. Shell finite elements based on the degeneration from the three-dimensional solid are considered [Ahmad et al., 1970]. The shear and membrane locking phenomena related to these elements are overcome by using the Mixed Interpolation of Tensorial Components (MITC) proposed by Bathe and co-workers. The MITC9 shell finite element [Bucalem and Bathe, 1993] is used in this work. The equilibrium equation for a given shell finite element l can be written as:

$$\tilde{\mathbf{K}}^{(l)} \mathbf{a}^{(l)} - \mathbf{Q}^{(l)} \mathbf{t}^{(l)} = \mathbf{f}^{(l)} \quad (7)$$

153 where $\tilde{\mathbf{K}}^{(l)} = \mathbf{K}^{(l)} - \omega^2 \mathbf{M}^{(l)}$ is the resulting time harmonic stiffness matrix, $\mathbf{a}^{(l)}$ is the vector of nodal displacements and rotations, $\mathbf{Q}^{(l)}$ is the matrix transferring distributed mid-surface load $\mathbf{t}^{(l)}$ to nodal loads, and $\mathbf{f}^{(l)}$ is the
 154 vector of equilibrating nodal forces.
 155

A conforming mesh between the crack-like boundary and the shell mid-surface is considered. Then, the coupling is performed by imposing perfectly welding conditions through the following compatibility and equilibrium between shell finite element and crack-like boundary:

$$u_k^+ = u_k^- = u_k^l \quad (8a)$$

$$t_k^+ + t_k^- + t_k^l = 0 \quad (8b)$$

156 where u_k^l denotes the shell displacements and t_k^l the distributed mid-surface shell load.

The seismic input is included in the formulation by following the classical decomposition of the total field into the superposition of the incident field (produced by the impinging seismic excitation) and the scattered field (produced by the foundation), see e.g. [Domínguez, 1993]:

$$u_k^{\text{tot}} = u_k^{\text{in}} + u_k^{\text{sc}} \quad (9a)$$

$$t_k^{\text{tot}} = t_k^{\text{in}} + t_k^{\text{sc}} \quad (9b)$$

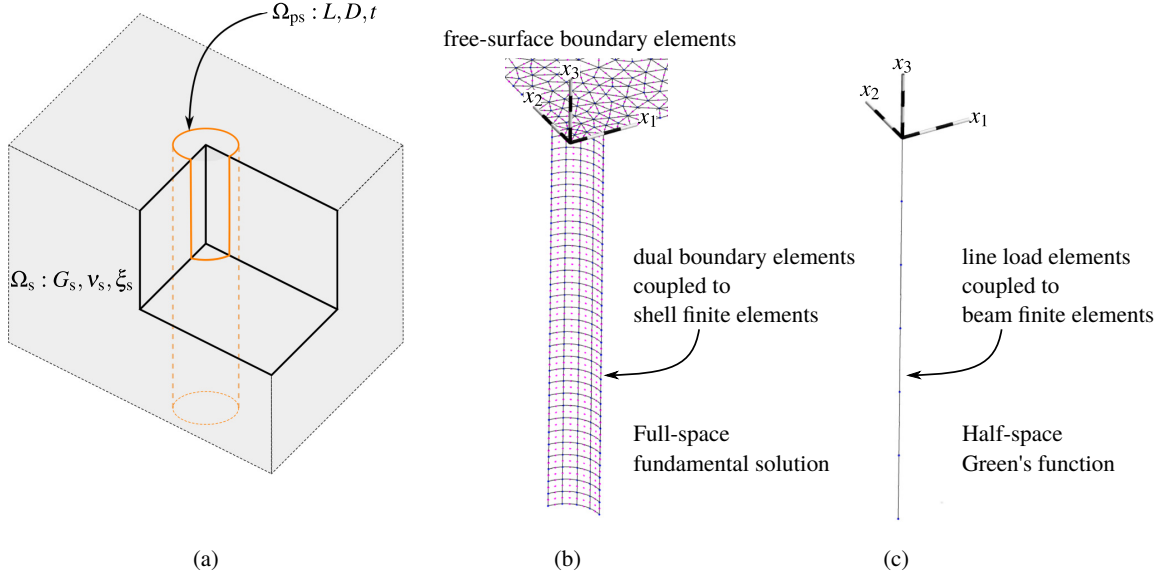


Figure 2: Foundation configuration and its modelling: (a) steel hollow pile in homogeneous half-space, (b) DBEM-FEM model [Bordón et al., 2017] (soil-shell interaction), (c) Integral model [Álamo et al., 2016] (soil-beam interaction)

Since the displacements and tractions present in the BIEs have to be evanescent, they are substituted by the scattered field, which, under the previous assumption, is equivalent to subtracting the incident field from the total field. The considered incident field is a simple vertically incident shear wave, which has the following non-zero displacements and tractions:

$$u_1^{\text{in}} = \frac{1}{2} \left(e^{-ik_s x_3} + e^{ik_s x_3} \right) \quad (10a)$$

$$t_1^{\text{in}} = G_s u_{1,3}^{\text{in}} n_3 \quad (10b)$$

$$t_3^{\text{in}} = G_s u_{1,3}^{\text{in}} n_1 \quad (10c)$$

157 where $k_s = \omega/c_s$ is the S wavenumber, $c_s = \sqrt{G_s^*/\rho_s}$ is the shear wave velocity, n_j is the unit normal at the
 158 boundary point, and $e^{i\omega t}$ has been omitted for brevity.

159 2.3 Soil-beam model

160 For a further reduction in the number of degrees of freedom of the problem, the monopile shaft or suction
 161 caisson skirt can be simplified to a unidimensional beam element. By doing so, the soil-foundation interface
 162 is concentrated into the beam axis and the behaviour at each point of the foundation element is defined by the
 163 cross-section displacements and rotations and the resultant of the interaction tractions along the ring. Evidently,

164 this kind of model is not able to capture the local effects produced at the soil-shell interface, but they can
 165 accurately approximate the global response of the foundation (especially for medium-to-large aspect ratios).

166 A numerical model with these features was proposed by the Authors in a previous work [Álamo et al., 2016]
 167 for the analysis of pile foundations. In addition to the reduction in the number of degrees of freedom achieved
 168 by the omission of the soil-shell interface, the developed model makes use of Green's functions for the layered
 169 half space instead of the previous full-space fundamental solution. Thus, the discretization of the soil free-
 170 surface and any strata interface is avoided as the Green's functions already satisfy the boundary conditions of
 171 those contours. As result, an efficient numerical model is obtained in which the only variables correspond to
 172 the mid-line of the foundation element. In the following, the basis of the model formulation are outlined. For a
 173 more detailed description, the original work [Álamo et al., 2016] is referred.

174 The soil region Ω_s is assumed to be formed by, in general, a group of horizontal layers overlying a half space.
 175 The presence of the foundation element is represented through a load line Γ_b over which the distributed soil-
 176 foundation interaction forces act, being these the only body forces in the soil domain. Due to the treatment of the
 177 foundation as a load line, the only boundary of the soil domain correspond to the free-surface Γ_{fs} . Considering
 178 that its zero-traction boundary condition is already satisfied by both the Green's functions and the unknown
 179 state, the Singular BIE for internal points of the soil domain can be reduced to:

$$u_l^i = \int_{\Gamma_b} \tilde{u}_{lk}^* q_k d\Gamma_b \quad (11)$$

180 where \tilde{u}_{lk}^* is the displacement Green's function for the layered half space proposed by Pak and Guzina
 181 [Pak and Guzina, 2002] and q_k are the distributed interaction forces acting over the soil. In order to numerically
 182 evaluate the line integral, classic lineal (2 nodes) elements are considered. Also, a particular non-nodal collocation
 183 strategy over four points of the fictitious soil-shell interface is required in order to avoid the singularity of
 184 the Green's function (see [Álamo et al., 2016] for more details).

The finite element modelling of the foundation piece is done by using two-noded beam elements. Cubic and
 quadratic shape functions that satisfy the Timoshenko's beam static equation [Friedman and Kosmatka, 1993]
 are used for the lateral behaviour, while linear shape functions are used to model the distributed interaction
 forces and axial displacements. The equilibrium equation for a given beam element l can be written as:

$$\tilde{\mathbf{K}}^{(l)} \mathbf{a}^{(l)} - \mathbf{Q}^{(l)} \mathbf{q}^{(l)} = \mathbf{f}^{(l)} \quad (12)$$

185 Note that the terms of this equation are the beam-counterparts of the ones presented in Eq. (7), being $\mathbf{q}^{(l)}$ the
 186 vector defining the nodal values of the distributed interaction forces acting over the foundation element.

Conforming meshes are considered to discretize the soil load line and the foundation element. Thus, the coupling between both regions can be easily done by, again, imposing compatibility and equilibrium conditions in terms of displacements and interaction forces, respectively:

$$u_k = u_k^l \quad (13a)$$

$$q_k + q_k^l = 0 \quad (13b)$$

187 where u_k^l denotes the beam displacements and q_k^l the distributed interaction forces acting over the beam.

188 Finally, and following the same strategy than in the previous soil-shell model, the seismic excitation is
 189 introduced by superposing the incident and scattered fields. Note that, owing to the reduced expression of the
 190 Singular BIE, in the soil-beam model only the displacement terms of the incident field are necessary.

191 3 Results and discussion

192 In this section, a comprehensive comparative study between results from both models is given. It includes
 193 the necessary ingredients for comparing the foundation characterization (impedances and kinematic interaction
 194 factors) as well as the final OWT variables of interest (bending moments, shear forces, displacements and
 195 rotations).

196 The study covers the following parameters: length to diameter ratio: $L/D = \{1, \dots, 10\}$, thickness to di-
 197 ameter ratio: $t/D = \{0.001, 0.01, 0.02\}$, and foundation shear modulus to soil shear modulus ratio: $G_f/G_s =$
 198 $\{1000, 4000, 16000\}$.

199 For this class of foundations in homogeneous soils this set of parameters completely defines the problem.
 200 Nonetheless, Doherty et al. [Doherty et al., 2005] found that the relative stiffness between the foundation lat-
 201 eral shell (bucket skirt or pile shaft) and the soil can effectively be synthesized via a dimensionless parameter
 202 $J_{\text{Doherty}} = (E_f t)/(G_s R)$ which relates shell membrane stiffness and soil stiffness (E_f is the Young's modulus of
 203 the foundation and R is the radius of the foundation cross-section). It allows an approximate but useful reduc-
 204 tion of the number of defining parameters. For convenience's sake, this dimensionless parameter is defined
 205 as $J = (G_f t)/(G_s D)$ in the present paper, which differs from the original by the factor $J_{\text{Doherty}}/J = 4(1 + \nu_f)$
 206 (constant since $\nu_f = 0.25$ in all cases). Although the work of Doherty et al. [Doherty et al., 2005] is limited to
 207 static stiffnesses, it is shown in Appendix A that, in general, J remains as a useful parameter in dynamics for

208 frequencies $a_o = fD/c_s < 0.3$ and $t/D \leq 0.05$.

209 The rest of dimensionless parameters that define the studied problems are: hysteretic damping ratios of
210 foundation $\xi_f = 2\%$ and soil $\xi_s = 5\%$ materials, foundation soil density ratio $\rho_f/\rho_s = 3.9$, and soil Poisson's
211 ratio $\nu_s = 0.49$ (saturated soil).

212 3.1 Static stiffnesses

213 Static stiffnesses are relevant for the calculation of the fundamental frequency of OWTs since it is usually small,
214 typically $f_1 \sim 0.3$ Hz [Kaynia, 2018]. For seismic analyses, however, the use of static stiffnesses is generally
215 not recommended.

216 Fig. 3 shows the vertical, horizontal, rocking and sway-rocking cross-coupling stiffness components for
217 most of the cases studied. One case per t/D has been removed since they have similar values of J (and similar
218 graphs) to other cases. This way, the stiffness components are distributed along columns, and the relative
219 stiffnesses between foundation and soil are distributed along rows. Each graph shows L/D in abscissas, and
220 contains the results from both models. In addition to the aforementioned Poisson's ratio $\nu_s = 0.49$ (saturated
221 soil), a value of $\nu_s = 0.3$ has been also considered in this section because the soil is expected to behave more
222 similar to the drained solid in the static regime. However, the influence of the Poisson's ratio in the comparison
223 between the two models is negligible. The beam model leads to similar results to the shell model except for very
224 small values of J . This phenomenon is reasonable since the validity of the beam-soil continua is kept as long as
225 the foundation behaves as a structural member, which happens when there exists stiffness contrast between this
226 element and the soil. On the other hand, the applicability of the beam model regarding the length to diameter
227 ratio (L/D) is surprisingly good even at $L/D = 1$.

228 In order to give a measure of the fidelity of the soil-beam model, the relative error between both models is
229 given in Fig. 4. Each graph has now the parameter J in abscissas, so that all different cases of t/D and G_f/G_s
230 are represented. Each length to diameter ratio is represented using a different color: $L/D = 2$ (black), $L/D = 4$
231 (red), $L/D = 6$ (blue), $L/D = 8$ (green) and $L/D = 10$ (orange); and each thickness to diameter ratio is shown
232 with a different point type: $t/D = 0.001$ (plus), $t/D = 0.01$ (cross) and $t/D = 0.02$ (square). In all cases, it
233 is roughly observed that error decreases as J increases, except for rocking and sway-rocking cross-coupling
234 stiffnesses for $L/D = 2$. The vertical stiffness shows a gradual reduction of the error as L/D increases, whereas
235 the lateral mode stiffnesses show little differences in the behaviour for $L/D \geq 4$. Overall, the beam model
236 achieves errors below 5% for the lateral mode stiffnesses and errors below 10% for the vertical stiffness when
237 $J \geq 10$ and $L/D \geq 4$.

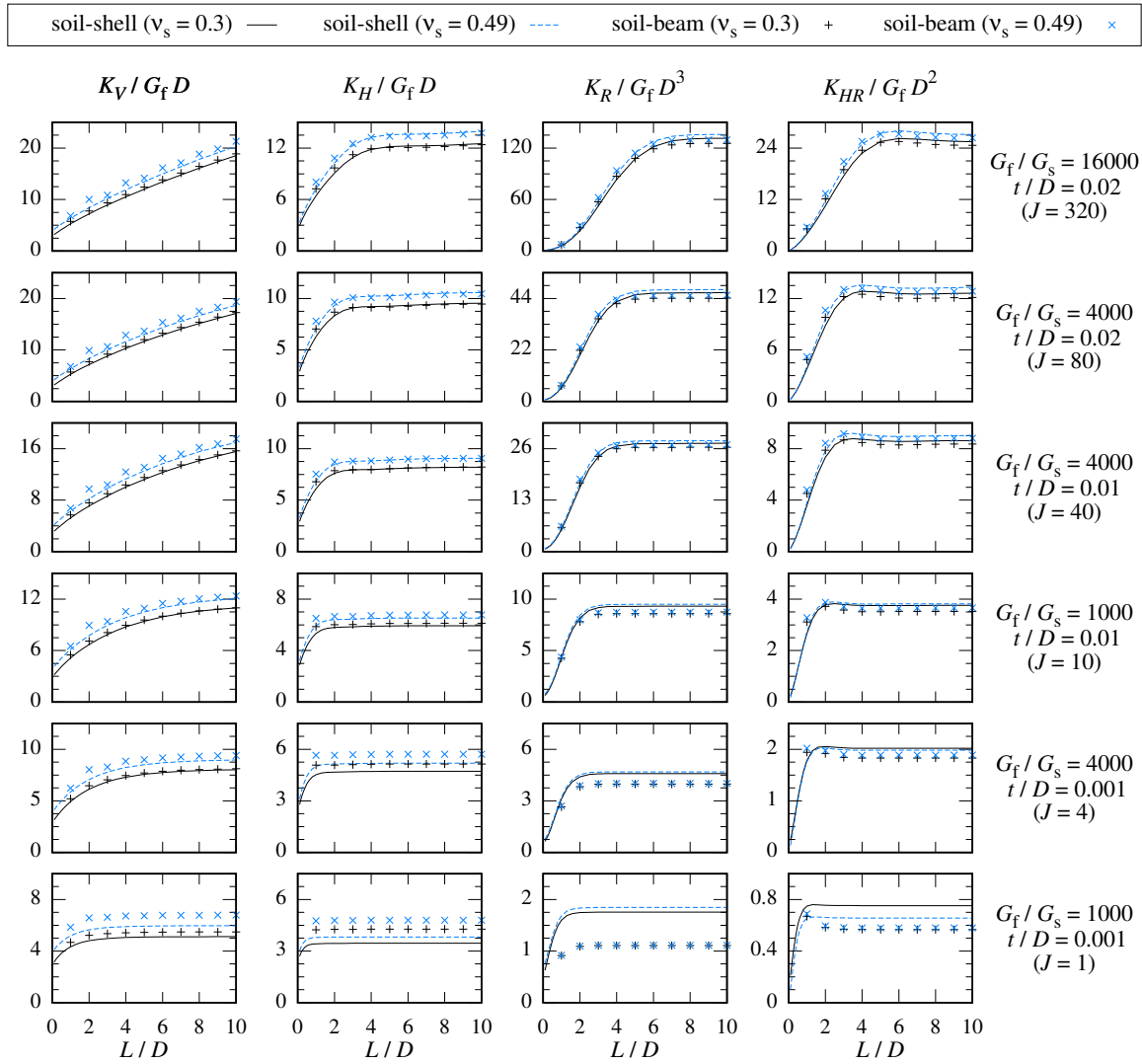


Figure 3: Comparison between static stiffnesses

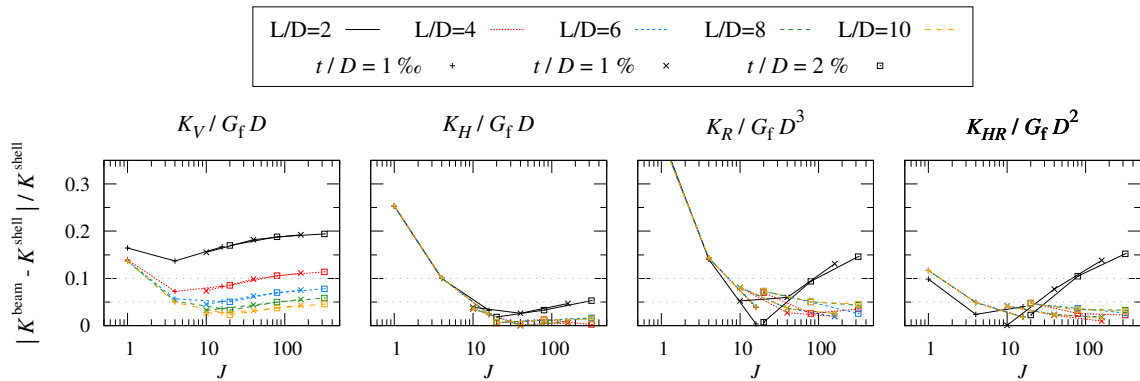


Figure 4: Relative errors for static stiffnesses ($\nu_s = 0.49$)

3.2 Impedance functions

The use of dynamic stiffnesses (also known as impedance functions) allows a much more general linear SSI analysis. They can be used for the calculation of OWT natural frequencies, as well as seismic analyses via the substructuring procedure. In this section, the comparison between beam and shell models is extended to impedance functions. The frequency-dependent differences between the two models are quantified through the relative error defined in Eq. (14). The proposed expression compares the absolute value of the complex difference between the result X obtained by the shell or beam approaches with respect to the maximum value obtained by the reference model (i.e., soil-shell approach) in the studied frequency range. This definition is preferred over a frequency-by-frequency relative comparison in order to avoid peak values of the error around the frequencies in which the reference result approaches to zero.

$$\Delta(a_o) = \frac{|X^{\text{beam}}(a_o) - X^{\text{shell}}(a_o)|}{\max_{a_o \in [0, 0.5]} [X^{\text{shell}}(a_o)]} \quad (14)$$

Fig. 5 shows the impedance curves (real and imaginary parts) as well as the relative error for the illustrative case with $L/D = 6$, $t/D = 0.01$ and $G_f/G_s = 4000$, i.e. $J = 40$. All other cases are included as supplementary data. For all stiffness components, the error between the beam and the shell models is approximately constant initially, and then it starts to increase with the frequency. Such effect is physically justifiable in terms of the comparison between soil wavelength and foundation diameter. For frequencies leading to wavelengths comparable to the foundation diameter, the reduction to a load line performed by the beam model becomes inadequate. Thus, it is reasonable that this model starts to fail beyond a quarter-wavelength per diameter ($a_o \geq 0.25$). In order to give a more concise measure of this limiting frequency, two limiting frequencies $a_{o,5\%}^{\text{lim}}$ and $a_{o,10\%}^{\text{lim}}$ are defined when the error reaches respectively 5 and 10 per cent.

Fig. 6 shows the values of $a_{o,5\%}^{\text{lim}}$ and $a_{o,10\%}^{\text{lim}}$ (calculated as in the previous illustrative case) for all cases under study. The line and point styles are also similar to the preceding section. The previously mentioned limit of $a_o \geq 0.25$ (associated with a quarter-wavelength per foundation diameter) is a valid indicative value for obtaining errors below 5%, although only when $J \geq 10$. In the vertical and rocking components, some $a_{o,5\%}^{\text{lim}}$ are located below 0.2. This erratic behaviour is nonetheless due to the presence of a peak in the beginning of these error curves which lightly exceed the 5% (see supplementary data). This is further demonstrated by observing that $a_{o,10\%}^{\text{lim}}$ do not show this behaviour.

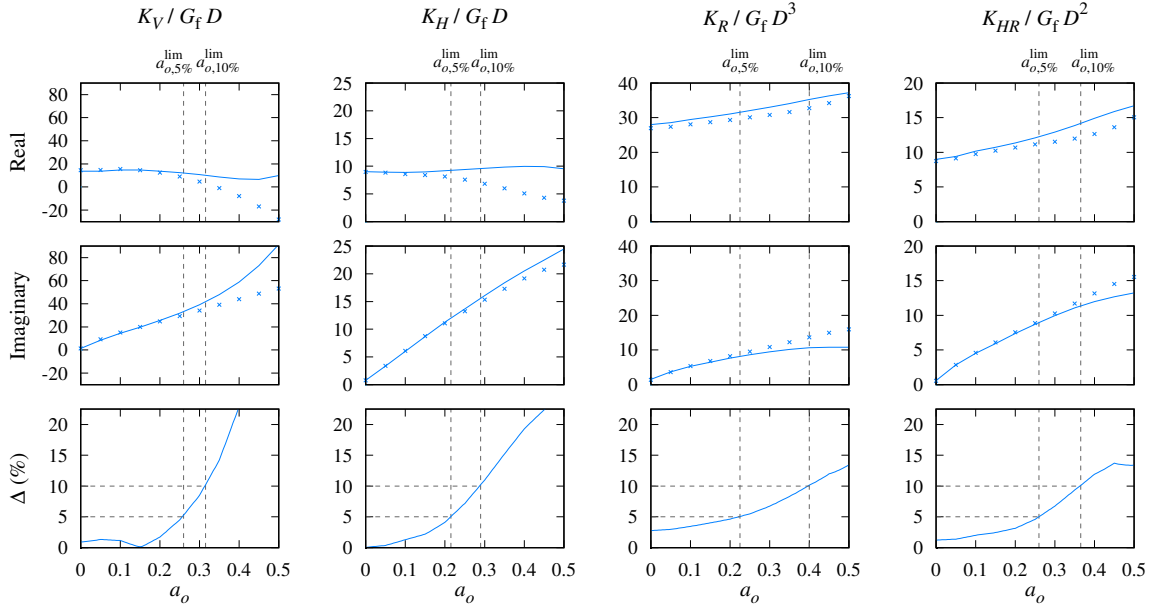


Figure 5: Comparison between dynamic stiffnesses: $L/D = 6$, $t/D = 0.01$ and $G_f/G_s = 4000$ ($J = 40$)

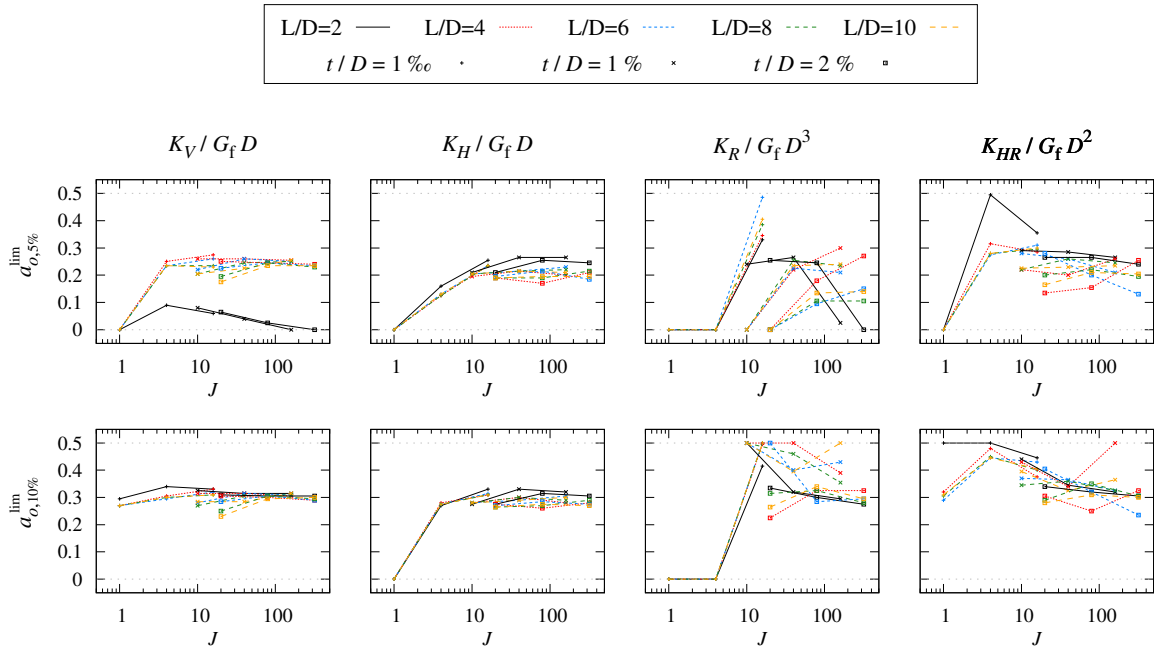


Figure 6: Limiting frequencies $a_{o,5\%}^{\lim}$ (error < 5%) and $a_{o,10\%}^{\lim}$ (error < 10%) of dynamic stiffnesses

264 3.3 Kinematic interaction factors

265 In this section, the discrepancies between both models are studied for the kinematic interaction factors I_u and
 266 I_θ (foundation with unrestrained head). These represent the filtering produced by the foundation in terms of
 267 displacements and rotations at the head of the foundation ($z = 0$) when subjected to an incident wave field. In
 268 this case, the study is limited to vertically incident shear waves, which are typically the most relevant ones.

269 Fig. 7 shows the kinematic interaction factors I_u and I_θ (real and imaginary parts) as well as the relative
 270 error (defined as in the previous section) for the illustrative case with $L/D = 6$, $t/D = 0.01$ and $G_f/G_s = 4000$,
 271 i.e. $J = 40$. All other cases are included as supplementary data. A good agreement between both models is
 272 observed, although higher discrepancies in the form of horizontal translation appear as the frequency increases.
 273 Thus, the error curves not only increase with the frequency, but also show several peaks and valleys. As in the
 274 case of impedance functions, it is possible to define two limiting frequencies $a_{o,5\%}^{\text{lim}}$ and $a_{o,10\%}^{\text{lim}}$ when the error
 275 reaches respectively 5 and 10 per cent.

276 Fig. 8 shows the values of $a_{o,5\%}^{\text{lim}}$ and $a_{o,10\%}^{\text{lim}}$ for all cases under study. The limiting frequencies are
 277 roughly $a_{o,5\%}^{\text{lim}} \sim a_{o,10\%}^{\text{lim}} \sim 0.1$ for $L/D = 2$, whereas for $L/D > 2$ and $J > 10$ these are $a_{o,5\%}^{\text{lim}} \sim 0.1 \div 0.2$ and
 278 $a_{o,10\%}^{\text{lim}} \sim 0.15 \div 0.5$. There is no clearly defined trend for the limiting frequencies due to the presence of the
 279 previously mentioned peaks. Nonetheless, it is reasonable to use the conventional quarter-wavelength limiting
 280 frequency ($a_o^{\text{lim}} = 0.25$) for the integral model regarding kinematic interaction factors, which achieves errors up
 281 to approximately 10% for $L/D > 2$ and $J > 10$.

282 3.4 Expressions for the limiting frequencies

From the results presented in the previous sections, ready-to-use formulas are obtained in order to estimate the
 limiting frequencies that ensure a certain error when using the beam model. A quadratic polynomial in terms
 of the logarithm of the foundation-soil relative stiffness parameter J is assumed for approximating the limiting
 frequencies:

$$a_{o,e}^{\text{lim}} \approx c_0 + c_1 \log J + c_2 (\log J)^2 \quad (15)$$

283 Tables 1 and 2 give the values of coefficients c_i for the two maximum errors of 5% and 10% respectively.
 284 Expressions are presented for all impedance functions and kinematic interaction terms with the exception of the
 285 sway-rocking cross-coupling impedance. This component is not included as it is generally less restrictive than
 286 either the lateral or rocking impedances (making no sense to use the former without the latter). Note that linear

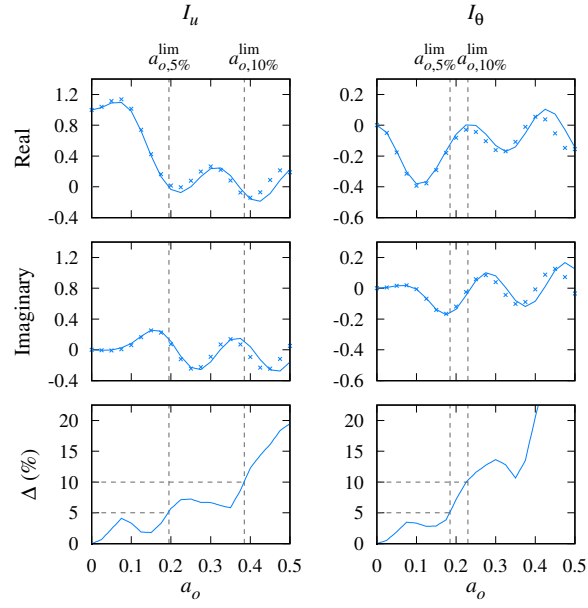


Figure 7: Comparison between kinematic interaction factors: $L/D = 6$, $t/D = 0.01$ and $G_f/G_s = 4000$ ($J = 40$)

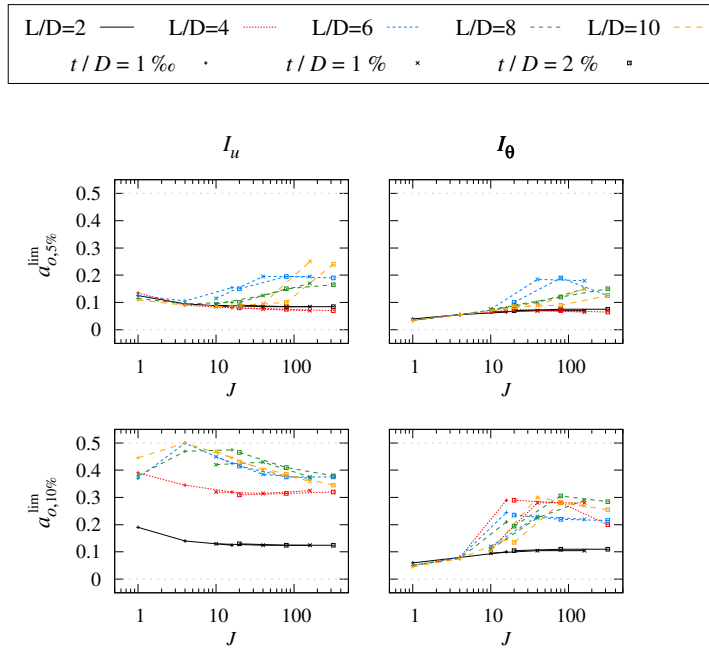


Figure 8: Limiting frequencies $a_{o,5\%}^{\text{lim}}$ (error <5%) and $a_{o,10\%}^{\text{lim}}$ (error <10%) of kinematic interaction factors

	c_0	c_1	c_2	Not applicable for
K_V	0.2584	-0.0332	0.0054	$J < 4, L/D < 4$
K_H	0.0322	0.0881	-0.0111	$J < 4$
K_R	1.2758	-0.4636	0.0455	$J < 16, L/D < 4, G_f/G_s < 4000$
I_u	0.1135	-0.0282	0.0065	$L/D < 6$ (use $a_o^{\text{lim}} \approx 0.084$)
I_θ	0.0343	0.0157	0	$L/D < 6$ (use $a_o^{\text{lim}} \approx 0.066$)

Table 1: Coefficients for the expressions of the limiting frequencies. Error $< 5\%$.

	c_0	c_1	c_2	Not applicable for
K_V	0.2664	0.0041	0	-
K_H	0.2760	0	0	$J < 4$
K_R	0.9667	-0.2693	0.0262	$J < 10, G_f/G_s < 4000$
I_u	0.5248	-0.0462	0.0026	$L/D < 6$ (use $a_o^{\text{lim}} \approx 0.13$ [$L/D = 2$] or 0.32 [$L/D = 4$])
I_θ	0.0414	0.0335	0	$L/D < 4$ (use $a_o^{\text{lim}} \approx 0.10$)

Table 2: Coefficients for the expressions of the limiting frequencies. Error $< 10\%$.

287 ($c_2 = 0$) or constant ($c_1 = c_2 = 0$) expressions are preferred when they can be used without a significant loss in
288 accuracy with respect to the quadratic formula.

289 The expressions provided by Tables 1 and 2 are not recommended for values of J outside the studied interval
290 $[1, 400]$. Also, for some components, the proposed formulas are not adequate for certain limit scenarios (such
291 as low foundation-soil stiffness contrast), which are indicated in the last column of each table. The proposed
292 formulas (lines) together with the previous results (points) are shown in Fig. 9. In each graphical area, the
293 limiting frequency is plotted against the dimensionless parameter J . Each column corresponds to a different
294 foundation variable, while each row corresponds to a different maximum permitted error. Note that the points
295 outside the applicability range of the obtained expressions are not included in the figure. For the kinematic
296 interaction factors, the alternative values for the points outside the applicability range are also shown in red and
297 purple colours.

298 3.5 Application example

299 In order to illustrate the accuracy of the soil-beam model to reproduce the response of the OWT-foundation
300 system, a practical example is briefly presented in this section. The system is based on the reference NREL-
301 5MW OWT model [Jonkman et al., 2009]. The tower is 70 m high and it has a hollow cross-section with
302 variable diameter from 6 m at its base to 3.87 m at the hub height, whereas a constant thickness to diameter
303 ratio of 0.45% is assumed. The supporting structure is a 20 m high, 6 m diameter and thickness ratio of 1%
304 tubular member. No transition piece between supporting structure and tower is considered in the analyses. The
305 foundation presents the same diameter ($D = 6$ m) and thickness ratio ($t/D = 1\%$) as the supporting structure.

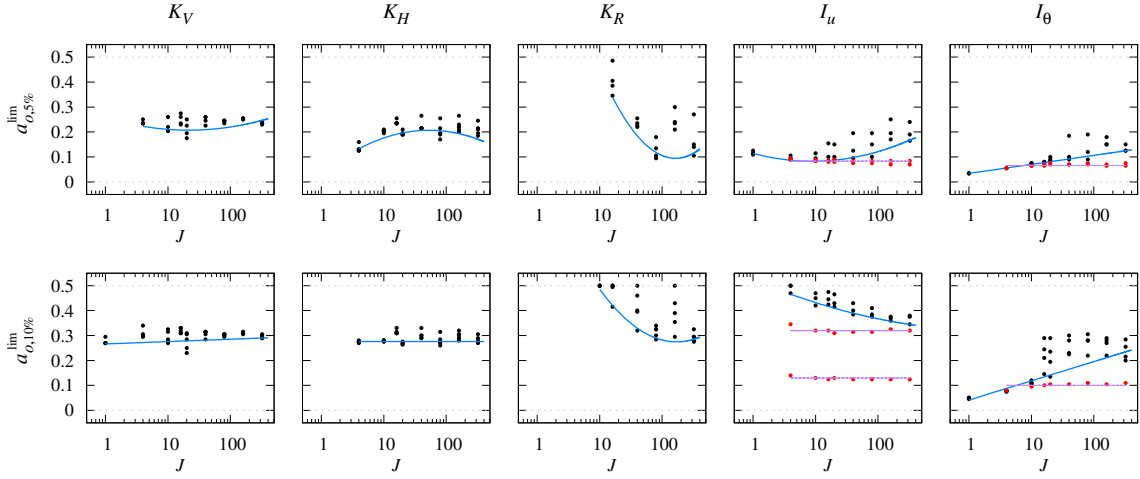


Figure 9: Comparison between the obtained limiting frequencies (points) and their proposed expressions (lines).

306 An intermediate embedment length ratio $L/D = 6$ is assumed in this example. The whole structure (tower,
 307 supporting monopile and foundation) is considered to be made of steel with: Youngs modulus $E_f = 210$ GPa,
 308 density $\rho_f = 7850$ kg/m³ and Poissons ratio $\nu_f = 0.25$. For the superstructure a hysteretic damping coefficient
 309 $\xi_f = 2.5\%$ is considered.

310 The soil properties are selected in order to reproduce a saturated media through elastic equivalent proper-
 311 ties: density $\rho_s = 2000$ kg/m³, Poissons ratio $\nu_s = 0.49$ and hysteretic damping coefficient $\xi_s = 5\%$. Different
 312 foundation-soil stiffness ratios $J = 10, 40$ and 160 are assumed in order to cover the range studied in the previ-
 313 ous sections. These values correspond to soils whose shear wave velocities are approximately $c_s = 200, 100$ and
 314 50 m/s, respectively.

315 In coherence with the obtained kinematic interaction factors, the considered seismic excitation is a vertically
 316 incident shear wave. The free-field displacement is denoted as u_{ff} , while its acceleration is \ddot{u}_{ff} .

317 Figure 10 shows the Frequency Response Functions (FRF) of several representative variables of the OWT
 318 system. The second and third rows present the FRF of the displacement and rotation atop the turbine tower
 319 with respect to the free-field displacement. On the other hand, the fourth and fifth rows illustrate the shear
 320 force and bending moment at the base of the supporting structure (mud-line level) with respect to the free-
 321 field acceleration. The results obtained by assuming a fixed-base model (no SSI) are compared with the ones
 322 obtained through the substructuring procedure (see Section 2.1) using both the soil-shell or soil-beam models
 323 to characterize the foundation. In order to help in interpreting the results, the first row shows the limiting
 324 frequencies (corresponding to a maximum relative error between the shell and beam models less than 10%) for
 325 all of the foundation variables involved in the problem at hand. Each column of the figure corresponds to a

326 different soil-foundation relative stiffness ratio. Frequencies up to 20 Hz are considered as a wide frequency
327 range for the energy content of the seismic excitation.

328 The results presented in Fig. 10 show a clear influence of the SSI effects on all studied variables. In general
329 terms, introducing the foundation behaviour results in a higher response of the system for small frequencies (<
330 5 Hz), and a lower response for higher frequencies. The shifting of the system natural frequencies toward lower
331 values produced by the SSI effects is also seen in the obtained results.

332 The accuracy of using the beam model instead of the shell one can be also tested by comparing their results
333 in Fig. 10. A good agreement between both models is found for all variables. Some discrepancies are pro-
334 duced for frequencies above certain limiting frequencies. The horizontal impedance term seems to be the most
335 important one, followed by the limit corresponding to the lateral kinematic interaction factor. However, these
336 differences between the soil-shell and soil-beam models are not significant for the example case studied (note
337 the logarithmic scale in the forces at the base variables). Thus, the results show that the real factor that limits
338 the use of the soil-beam model is the maximum value of the dimensionless frequency $a_o = 0.5$, i.e., foundation
339 diameter equal to half of the wavelength. This restriction makes the soil-beam model to be used with caution
340 for seismic analyses of large diameter foundations in extremely soft soils. The validity of the beam model in
341 this scenario will strongly depend on the frequency content of the excitation, and the evolution with frequency
342 of the studied FRF.

343 4 Conclusions

344 This paper presents a comparison between soil-shell and soil-beam models for the dynamic characterization of
345 OWT foundation elements (piles or suction caissons) and the seismic analysis of the complete system. The
346 reference results are computed with the first model, that uses Boundary Elements to model the soil behaviour
347 coupled with shell Finite Elements to represent the foundation element. On the other hand, the soil-beam model
348 is based on the integral expression of the Reciprocity Theorem together with advanced Green's functions for
349 the soil modelling, while the structural behaviour of the foundation is handled via beam Finite Elements. For
350 the analyses, soil and foundation geometrical and material properties typical of this singular construction are
351 assumed.

352 First, the comparison is made in terms of the foundation characterization variables: static stiffness, impedance
353 functions and kinematic interaction factors. A dimensionless analysis is made in order to present more general
354 results. The main conclusions drawn from this study are:

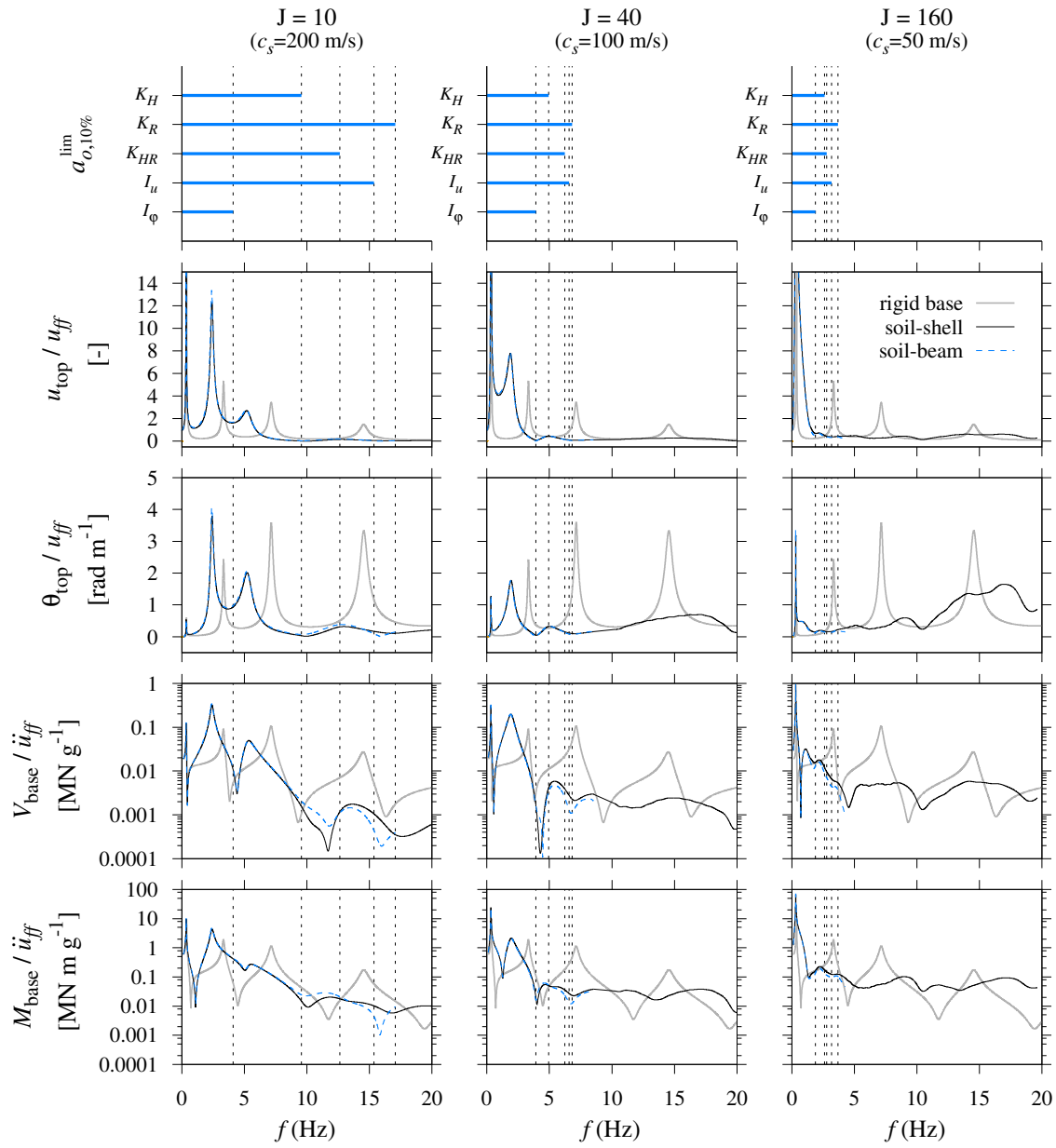


Figure 10: Frequency Response Functions for representative variables of the OWT system. Comparison between the different models.

- 355 • The dimensionless parameter J proposed by Doherty et al. [Doherty et al., 2005] to define the relative
356 stiffness between the foundation and soil in static can be also applied for dynamic analyses.
- 357 • In general terms, the soil-beam model accurately reproduces the global foundation response with respect
358 to the rigorous soil-shell model. The agreement is quite good even for foundations with small aspect
359 ratios.
- 360 • The accuracy of the beam model is reduced for high frequencies and low foundation-soil stiffness contrast.
- 361 • Closed-form expressions are proposed in order to estimate the applicability range, in terms of maximum
362 dimensionless frequency, of the beam simplification. Those are functions of the foundation-soil relative
363 stiffness parameter J and depend on the foundation variable to compute and maximum admissible error.

364 An application example is also presented, in which the seismic response of a 5 MW OWT including SSI
365 effects is computed via a substructuring procedure. The FRF of key structural variables obtained by both models
366 (shell and beam) are compared, and the main conclusions drawn from this example are the following:

- 367 • The soil-structure interaction effects significantly change the seismic response of the OWT system.
- 368 • The foundation variable whose modelling has more impact on the obtained results is the lateral impedance
369 term, followed by the lateral kinematic interaction factor.
- 370 • Below the proposed limiting frequencies, virtually the same results are obtained regardless using the beam
371 or shell model.
- 372 • Even above these limits, the foundation beam model accurately reproduces the OWT response in an
373 acceptable frequency range for seismic analyses. The upper bound corresponds to the frequency for
374 which the foundation diameter coincides with half wavelength.
- 375 • This restrains the use of the beam model for extremely soft soils if the high frequency content of the
376 excitation is important. But for typical scenarios, the foundation beam simplification is a valid option for
377 reproducing the OWT seismic response, making it a valuable tool especially for design or optimization
378 steps.

379 **Acknowledgements**

380 This work was supported by Agencia Estatal de Investigación (AEI) of Spain through research project BIA2017-
381 88770-R. J.D.R. Bordón is a postdoctoral fellow of the ULPGC Postdoctoral Programme. The authors are

382 grateful for this support.

383 **References**

384 [Ahmad et al., 1970] Ahmad, S., Irons, B. M., and Zienkiewicz, O. C. (1970). Analysis of thick and thin shell
385 structures by curved finite elements. *International Journal for Numerical Methods in Engineering*, 2(3):419–
386 451.

387 [Álamo et al., 2016] Álamo, G. M., Martínez-Castro, A. E., Padrón, L. A., Aznárez, J. J., Gallego, R., and
388 Maeso, O. (2016). Efficient numerical model for the computation of impedance functions of inclined pile
389 groups in layered soils. *Engineering Structures*, 126(1):379–390.

390 [Almeida and de Paiva, 2004] Almeida, V. S. and de Paiva, J. B. (2004). A mixed BEM-FEM formulation for
391 layered soil-superstructure interaction. *Engineering Analysis with Boundary Elements*, 28(9).

392 [Arany et al., 2017] Arany, L., Bhattacharya, S., Macdonald, J., and Hogan, S. J. (2017). Design of monopiles
393 for offshore wind turbines in 10 steps. *Soil Dynamics and Earthquake Engineering*, 92:126–152.

394 [Ariza and Domínguez, 2002] Ariza, P. and Domínguez, J. (2002). General BE approach for three-dimensional
395 dynamic fracture analysis. *Engineering Analysis with Boundary Elements*, 26:639–651.

396 [Ashuri et al., 2014] Ashuri, T., Zaijijer, M. B., Martins, J. R. R. A., van Bussel, G. J. W., and van Kuik, G.
397 A. M. (2014). Multidisciplinary design optimization of offshore wind turbines for minimum leveled cost
398 of energy. *Renewable Energy*, 68:893–905.

399 [Bhattacharya et al., 2013] Bhattacharya, S., Nikitas, N., Garnsey, J., Alexander, N. A., Cox, J., Lombardi, D.,
400 Wood, D. M., and Nash, D. F. T. (2013). Observed dynamic soil–structure interaction in scale testing of
401 offshore wind turbine foundations. *Soil Dynamics and Earthquake Engineering*, 54:47–60.

402 [Bordón et al., 2017] Bordón, J. D. R., Aznárez, J. J., and Maeso, O. (2017). Dynamic model of open shell
403 structures buried in poroelastic soils. *Computational Mechanics*, 60(2):269–288.

404 [Bordón et al., 2019] Bordón, J. D. R., Aznárez, J. J., Padrón, L. A., Maeso, O., and Bhattacharya, S. (2019).
405 Closed-form stiffnesses of multi-bucket foundations for OWT including group effect correction factors. *Ma-
406 rine Structures*, 65:326–342.

407 [Bucalem and Bathe, 1993] Bucalem, M. L. and Bathe, K. J. (1993). Higher-order MITC general shell ele-
408 ments. *International Journal for Numerical Methods in Engineering*, 36:3729–3754.

- 409 [Coda et al., 1999] Coda, H. B., Venturini, W. S., and Aliabadi, M. H. (1999). A general 3D BEM/FEM
410 coupling applied to elastodynamic continua/frame structures interaction analysis. *International Journal for*
411 *Numerical Methods in Engineering*, 46(5):695–712.
- 412 [Cotter, 2009] Cotter, O. (2009). *The installation of suction caisson foundations for offshore renewable energy*
413 *structures*. PhD thesis, University of Oxford - Magdalen College.
- 414 [DNV, 2014] DNV (2014). Offshore standard DNV-OS-J101: design of offshore wind turbine structures. Det
415 Norske Veritas.
- 416 [Doherty and Deeks, 2003] Doherty, J. P. and Deeks, A. J. (2003). Elastic response of circular footings embed-
417 ded in a non-homogeneous half-space. *Géotechnique*, 53(8):703–714.
- 418 [Doherty et al., 2005] Doherty, J. P., Houlsby, G. T., and Deeks, A. J. (2005). Stiffness of flexible caisson
419 foundations embedded in nonhomogeneous elastic soil. *Journal of Geotechnical and Geoenvironmental*
420 *Engineering*, 131(12):1498–1508.
- 421 [Domínguez, 1993] Domínguez, J. (1993). *Boundary Elements in Dynamics*. International Series on Compu-
422 tational Engineering. Computational Mechanics Publications.
- 423 [Domínguez et al., 2000] Domínguez, J., Ariza, M. P., and Gallego, R. (2000). Flux and traction boundary
424 elements without hypersingular or strongly singular integrals. *International Journal for Numerical Methods*
425 *in Engineering*, 48:111–135.
- 426 [Friedman and Kosmatka, 1993] Friedman, Z. and Kosmatka, J. B. (1993). An improved two-node Timoshenko
427 beam finite element. *Computers and Structures*, 47(3):473–481.
- 428 [Gazetas and Dobry, 1984] Gazetas, G. and Dobry, R. (1984). Horizontal response of piles in layered soils.
429 *Journal of Geotechnical Engineering*, 110(1):20–40.
- 430 [Houlsby and Byrne, 2005a] Houlsby, G. T. and Byrne, B. W. (2005a). Design procedures for installation of
431 suction caissons in clay and other materials. *Proceedings of the Institution of Civil Engineers*, 158(GE2):75–
432 82.
- 433 [Houlsby and Byrne, 2005b] Houlsby, G. T. and Byrne, B. W. (2005b). Design procedures for installation of
434 suction caissons in sand. *Proceedings of the Institution of Civil Engineers*, 158(GE3):135–144.
- 435 [Jia et al., 2018] Jia, N., Zhang, P., Liu, Y., and Ding, H. (2018). Bearing capacity of composite bucket foun-
436 dations for offshore wind turbines in silty sand. *Ocean Engineering*, 151:1 – 11.

- 437 [Jiménez-Salas and Belzunce, 1965] Jiménez-Salas, J. A. and Belzunce, J. A. (1965). Theoretical solution
438 of stress distribution in piles. In *Proceedings of the VI International Conference on Soil Mechanics and*
439 *Foundation Engineering*.
- 440 [Jonkman et al., 2009] Jonkman, J., Butterfield, S., Musial, W., and Scott, G. (2009). Definition of a 5-MW
441 Reference Wind Turbine for Offshore System Development. Technical Report NREL/TP-500-38060, Na-
442 tional Renewable Energy Laboratory.
- 443 [Kaynia and Kausel, 1982] Kaynia, A. and Kausel, E. (1982). Dynamic stiffness and seismic response of pile
444 groups. resreport R82-03, Massachusetts Institute of Technology.
- 445 [Kaynia, 2018] Kaynia, A. M. (2018). Seismic considerations in design of offshore wind turbine. *Soil Dynam-*
446 *ics and Earthquake Engineering*.
- 447 [Novak et al., 1978] Novak, M., Nogami, T., and Aboul-Ella, F. (1978). Dynamic soil reactions for plane strain
448 case. *Journal of the Engineering Mechanics Division (ASCE)*, 104:953–959.
- 449 [Padrón et al., 2007] Padrón, L., Aznárez, J., and Maeso, O. (2007). BEM-FEM coupling model for the dy-
450 namic analysis of piles and pile groups. *Engineering Analysis with Boundary Elements*, 31(6):473 – 484.
- 451 [Page et al., 2019] Page, A. M., Naess, V., de Vaal, J. B., Eiksund, G. R., and Nygaard, T. A. (2019). Impact
452 of foundation modelling in offshore wind turbines: comparison between simulations and field data. *Marine*
453 *Structures*, 64:379–400.
- 454 [Pak and Guzina, 2002] Pak, R. Y. S. and Guzina, B. B. (2002). Three-dimensional Green’s functions for a
455 multilayered half-space in displacement potentials. *Journal of Engineering Mechanics*, 128(4):449–461.
- 456 [Poulos and Davis, 1968] Poulos, H. G. and Davis, E. H. (1968). The settlement behaviour of single axially
457 loaded incompressible piles and piers. *Géotechnique*, 18:351–371.
- 458 [Thurman and D’Appolonia, 1965] Thurman, A. and D’Appolonia, E. (1965). Computed movement of friction
459 and end-bearing piles embedded in uniform and stratified soils. In *Proceedings of the VI International*
460 *Conference on Soil Mechanics and Foundation Engineering*, number 2, pages 323–327.

461 **A Validity of J as characteristic dimensionless parameter for dynamic** 462 **analyses**

463 The dimensionless parameter J was proposed by Doherty et al. [Doherty and Deeks, 2003] to characterize the
464 relative stiffness between the foundation and soil for static analyses. In this appendix, its use in dynamic regime
465 is tested by computing the impedance functions and kinematic interaction factors for several configurations and
466 comparing the results obtained for the same value of J .

467 Five shell thickness ratios $t/D = \{0.001, 0.01, 0.02, 0.05, 0.1\}$ are combined with a continuum range of
468 values for the ratio between the foundation and soil shear modulus G_f/G_s in order to cover a comparable J
469 interval. For brevity's sake, only results for a configuration with aspect ratio $L/D = 6$ are presented. The rest of
470 dimensionless properties are equal to the ones defined in Section 3.

471 Figure 11 plots the impedance functions against the parameter J for the studied configurations. Real and
472 imaginary components are presented in pairs for several dimensionless frequencies distributed in rows. Each
473 column correspond to different impedance modes. The results show that the parameter J can be used to represent
474 the relative foundation-soil stiffness for the static and low frequency scenarios. For higher frequencies the
475 results are sensible to the thickness ratio if its value is larger than 2%, especially the vertical and lateral modes.
476 However, the foundation elements for OWT structures typically present thickness ratios below this value, so the
477 parameter J can be safely used to represent the foundation-soil stiffness contrast.

478 Figure 12 shows now the results in terms of kinematic interaction factors. The real and imaginary com-
479 ponents of the lateral and rotational terms are presented in pairs of rows. Each column correspond to different
480 dimensionless frequencies (static values are omitted as their results are trivial). As commented before, for thick-
481 ness ratios below 5%, the behaviour of the different configuration is determined by the J parameter. Thus, it
482 can be also used to characterize the foundation-soil relative stiffness when studying the foundation kinematic
483 response.

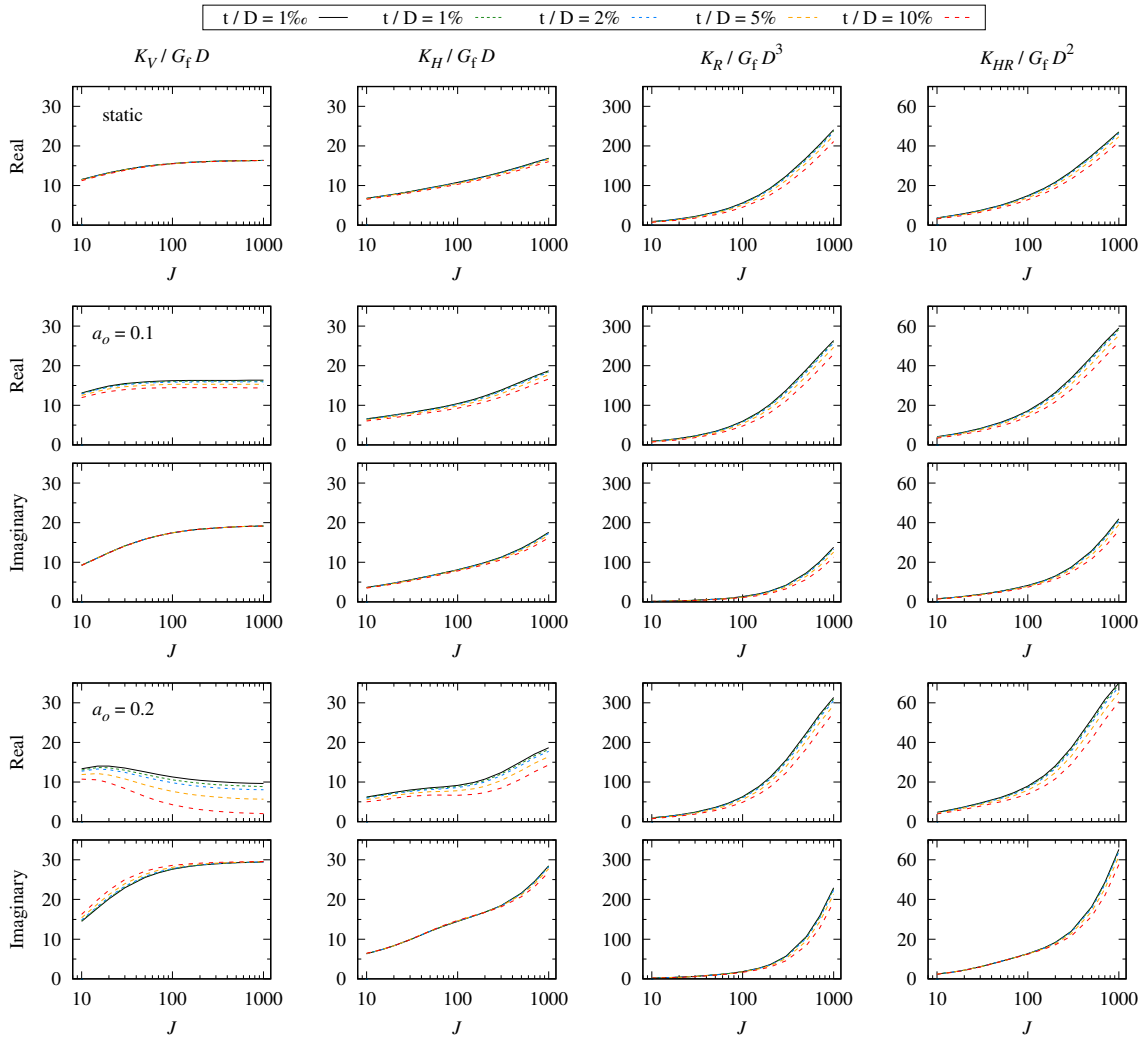


Figure 11: Validity of J for characterizing the relative foundation-soil stiffness in the computation of impedance functions.

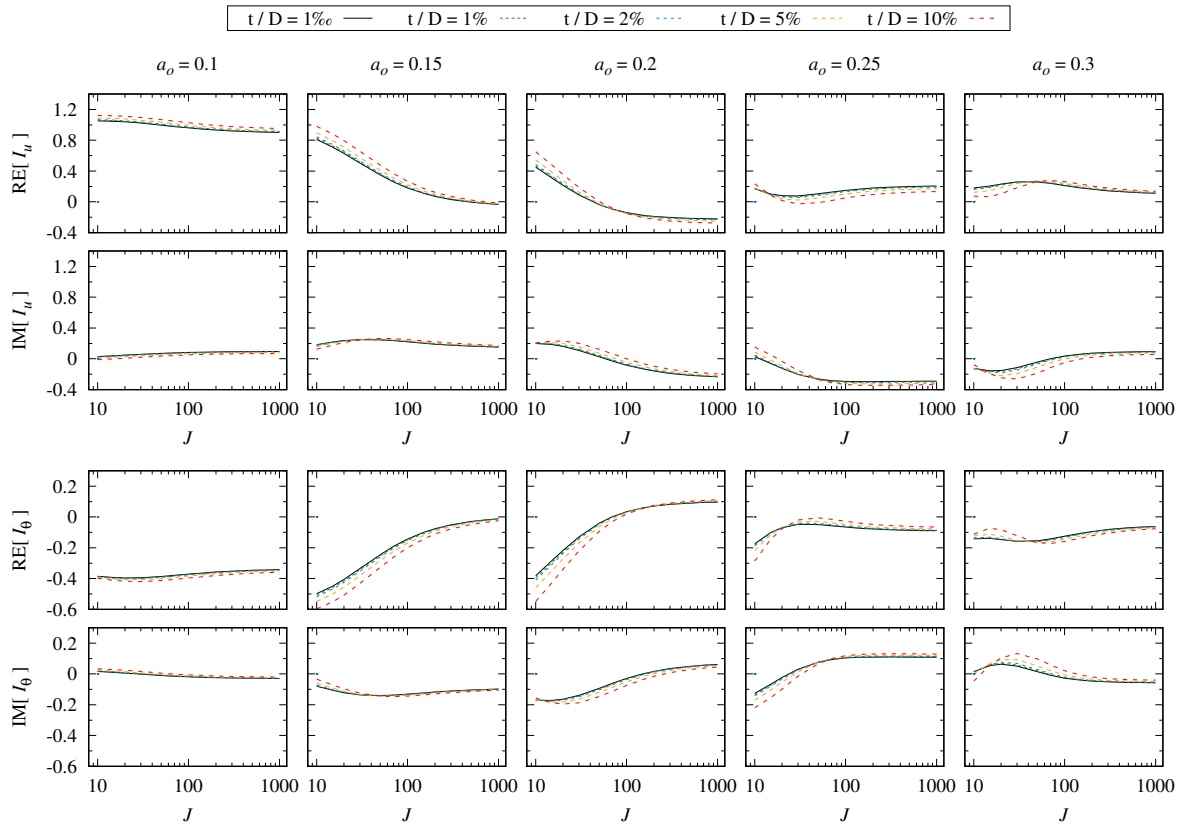


Figure 12: Validity of J for characterizing the relative foundation-soil stiffness in the computation of kinematic interaction factors.